



This is a repository copy of *Measuring the ocean wave directional spectrum`First Five' with HF radar.*

White Rose Research Online URL for this paper:  
<http://eprints.whiterose.ac.uk/138085/>

Version: Published Version

---

**Article:**

Wyatt, L.R. [orcid.org/0000-0002-9483-0018](https://orcid.org/0000-0002-9483-0018) (2019) Measuring the ocean wave directional spectrum`First Five' with HF radar. *Ocean Dynamics*, 69 (1). pp. 123-144. ISSN 1616-7341

<https://doi.org/10.1007/s10236-018-1235-8>

---

**Reuse**

This article is distributed under the terms of the Creative Commons Attribution (CC BY) licence. This licence allows you to distribute, remix, tweak, and build upon the work, even commercially, as long as you credit the authors for the original work. More information and the full terms of the licence here:

<https://creativecommons.org/licenses/>

**Takedown**

If you consider content in White Rose Research Online to be in breach of UK law, please notify us by emailing [eprints@whiterose.ac.uk](mailto:eprints@whiterose.ac.uk) including the URL of the record and the reason for the withdrawal request.



[eprints@whiterose.ac.uk](mailto:eprints@whiterose.ac.uk)  
<https://eprints.whiterose.ac.uk/>



# Measuring the ocean wave directional spectrum ‘First Five’ with HF radar

Lucy R. Wyatt<sup>1,2</sup>

Received: 25 February 2018 / Accepted: 31 October 2018  
© The Author(s) 2018

## Abstract

An ability to reliably measure the first five Fourier coefficients of the directional distribution of ocean wave energy is becoming an international requirement for any directional wave measurement device. HF radar systems are now commonly used for surface current measurement in the coastal ocean but robust wave measurements are more difficult to achieve. A number of HF radar deployments have demonstrated an ability to measure the directional spectrum, and in this paper, an evaluation of the Fourier coefficients derived from these spectra is presented. It is shown that, when data quality is good, good quality spectra and Fourier coefficients result. Recommendations for addressing some of the radar data quality issues that do arise are presented.

**Keywords** HF radar · Ocean wave directional spectrum · Fourier coefficient · First five · WERA · Pisces

## 1 Introduction

Ocean waves can sink ships and small boats, move sand and sediments, erode beaches and coastal defences, increase coastal flooding, and damage inshore, offshore and land-based structures. They can also provide power, help to break up oil and pollution slicks, and support marine activities such as surfing and fishing. In many of these cases, a measurement of waveheight alone is not sufficient; the directional and frequency (or equivalently period or wavelength) distribution of wave energy, known as the ocean wave directional spectrum, is important. For example, offshore

structures may have dangerous resonances at particular periods; beach erosion impacts will depend on the dominant wave directions during storms; marine renewable devices may have limited directional responses. As a result, many wave measuring devices now have spectral and directional measurement capabilities. In coastal regions, there are a number of factors, e.g. current shear, bottom and coastal topography, and sea breeze, that lead to spatial variations in wave properties. To capture this variability would require a big investment in buoys which in turn would provide increased hazards for shipping. Remote sensing from the coast using HF radars provides an opportunity to measure this spatial variability without any physical interference with offshore activities.

The ‘First Five’ refers to parameters of the ocean wave directional spectrum which include the energy spectrum,  $E(f)$ , and the first four Fourier coefficients,  $a_1, b_1, a_2, b_2$ , of the directional distribution of ocean waves at each wave frequency. These data are routinely provided by directional wave buoys and can also be used to provide measurements of directional spreading, skewness and kurtosis. Swail et al. (2010), in their comprehensive overview of wave measurements, conclude that “It is strongly recommended that all directional wave measuring devices should reliably estimate ‘First 5’ standard parameters and ‘First-5’ compliant

---

This article is part of the Topical Collection on the *15th International Workshop on Wave Hindcasting and Forecasting in Liverpool, UK, September 10–15, 2017*

---

Responsible Editor: Oyvind Breivik

✉ Lucy R. Wyatt  
l.wyatt@sheffield.ac.uk

<sup>1</sup> School of Mathematics and Statistics, University of Sheffield, Sheffield S10 2TN, UK

<sup>2</sup> Seaview Sensing Ltd., Sheffield, UK

is a priority both for operational and climate assessment requirements". This recommendation is also referred to in the IOOS wave observation plan (USACE 2009) and can be found on the JCOMM website so it would appear to have widespread international support. None of these sources provide specific guidance on what constitutes a reliable first five measurement. Accuracy requirements are usually given for just a few key parameters of the spectrum, e.g. significant waveheight, peak period and direction. Standards for first five measurement need to be developed and perhaps this paper will play a role in stimulating that work.

The measurement of waves with HF radar dates back to the 1970s; however, the development and success of the CODAR SeaSonde radar system focussed attention much more on the current measurement capabilities of HF radar. This is because it is much more difficult to get robust wave measurements from compact radars of this type although, in suitable circumstances, some wave parameters can be obtained (e.g. Long et al. 2011; Lipa et al. 2014). Phased array radars such as Pisces and WERA are much more suitable for directional spectrum measurements and the results from a number of trials demonstrating this capability have been published (e.g. Wyatt et al. 2003, 2006, 2011). This paper looks in particular at the accuracy of the 'First-5' obtained from HF radar measured directional spectra compared with those from directional wave buoys.

HF radar systems are normally located on the coast in pairs or, in some parts of the world, in interconnected networks, and measure backscatter from ocean waves of radio waves with a frequency in the HF band (3–30 MHz). The backscatter can be measured to ranges from the coast of up to 300 km when low HF frequencies are used, or up to 50 or so km at the higher HF frequencies. Maps of wave, current and wind measurements can be made with spatial resolutions from 250 m to 5 km or more again depending on the operating frequency, on antenna configuration and on available radio bandwidth.

The main scattering mechanism is Bragg scattering from linear ocean waves with half the radio wavelength travelling towards and away from the radar. These ocean waves propagate with speeds determined by the linear dispersion relationship and thus can be easily identified in the power spectrum (commonly referred to as the Doppler spectrum) of the backscattered signal from their frequency signature, i.e. they appear in the spectrum as high amplitude peaks at a frequency given by, in deep water,  $\sqrt{2gk_r}$  rad/s where  $g$  is gravitational acceleration and  $k_r$  is the radio wavenumber. These peaks are shifted in frequency if there is a surface current by the component of that current in the radar look direction and this additional shift is used to

determine that current component. Non-linear wave-wave interactions can also generate ocean waves with the Bragg scattering wavelength but these travel with different phase speeds and are thus separated from the scatter from linear waves because they have different frequency signatures. Double electromagnetic scattering from waves on the sea surface has a similar effect but in general is lower in amplitude in the Doppler spectrum than the hydrodynamic contribution.

The first theoretical formulation of the relationship between the backscattered power spectrum and the ocean wave directional spectrum was published by Barrick (1972a, b) and Barrick and Weber (1977). This took the form of an integral equation which can be broken down into first (linear waves)- and second (non-linear waves and double electromagnetic)-order terms. To obtain wave measurements, the second-order integral equation needs to be inverted and several attempts have been made to do that (e.g. Lipa 1977; Lipa and Barrick 1986; Wyatt 1990, 2000; Howell and Walsh 1993; Hisaki 1996; Hashimoto and Tokuda 1999; 2000; Green and Wyatt 2006). Another approach has been to develop empirical relationships between the Doppler spectrum or its integral and the ocean wave frequency spectrum or its parameters, e.g. significant waveheight. However, these empirical methods do not provide measurements of the Fourier coefficients so will not be discussed further here.

The nature of the integral equation puts some limits on the waveheight range that can be measured at a particular ocean wave frequency. This is illustrated in Fig. 1. The inversion process can only provide measurements at frequencies lower than the Bragg frequency. Taking the 10 MHz case, it can be seen that its Bragg frequency is too low to measure any waves at a waveheight of 0.2 m

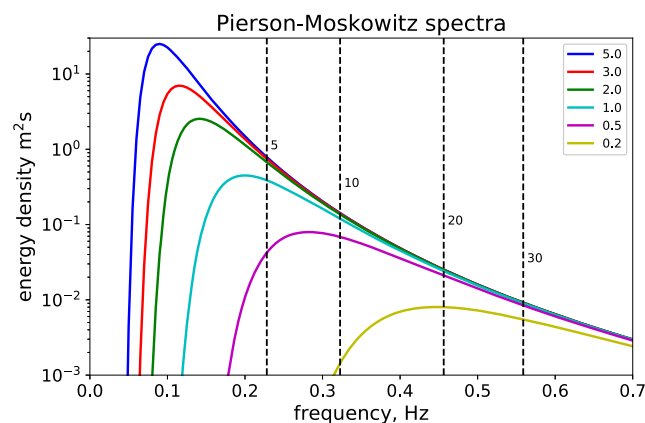
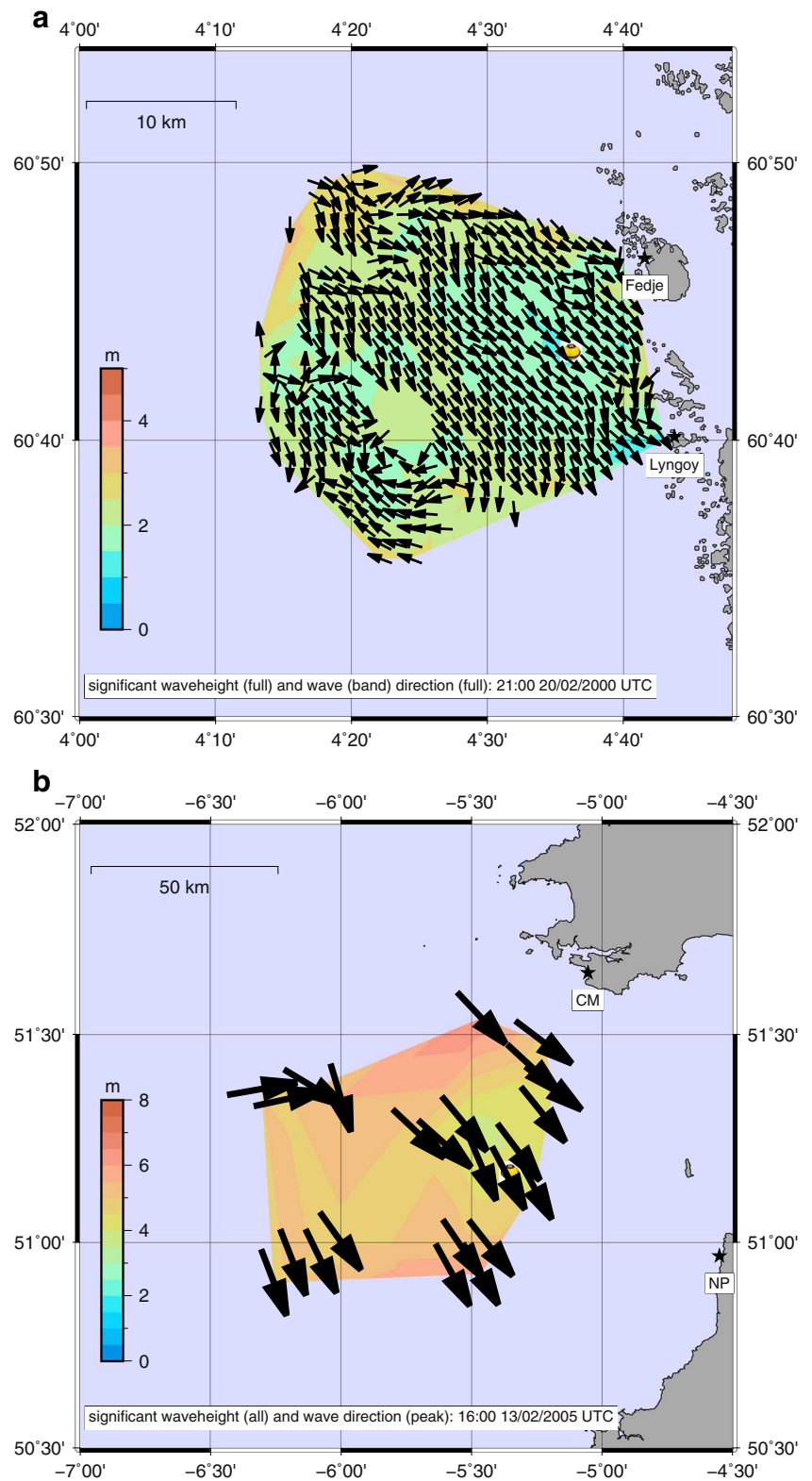


**Fig. 1** Pierson-Moskowitz spectra for different significant waveheights (in metres, colour coded). Vertical dashed lines indicate the Bragg frequencies for the radio frequencies (in MHz) shown

**Fig. 2** Significant waveheight and mean direction with WERA in Norway on 20/02/2000 @ 21:00 (above) and (below) significant waveheight and peak direction with Pisces in Celtic Sea on 13/02/2005 @ 16:00. Radar sites shown with ★. The buoy image marks position of the buoy



and is too close to the peak frequency at 0.5 m to get an accurate inversion. At a waveheight of 1.0 m, inversion is

just about feasible. At 30 MHz on the other hand when the waveheight is large, the linearisation approximation

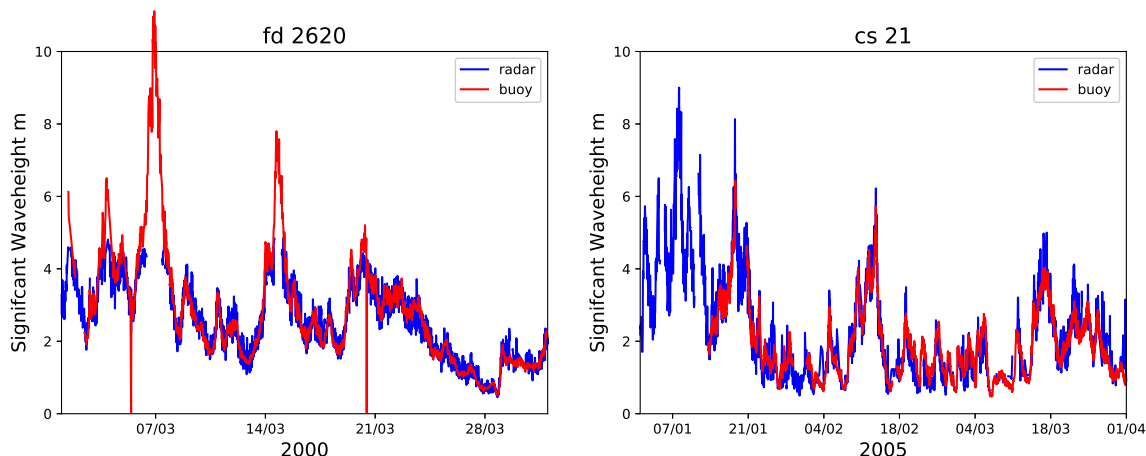


**Fig. 3** Significant waveheight comparisons for Norwegian (left) and the Celtic Sea (right) deployments. Radar measurement in blue, buoy in red

used in the development of the integral equation becomes increasingly unreliable, also it becomes much more difficult to separate first- from second-order parts of the Doppler spectrum (the Bragg waves are much lower in amplitude than the energy containing waves) and inversion fails.

The inversion method used to obtain the data presented in this paper (Wyatt 1990; Green and Wyatt 2006) provides the ocean wavenumber directional spectrum at each measurement location with sufficient second-order signal to noise. It is an iterative method, initialised with a Pierson-Moskowitz spectrum (Pierson and Moskowitz 1964) and a uni-modal  $\text{sech}^2$  directional model (Donelan et al. 1985) using an empirical model for the Pierson-Moskowitz waveheight (Wyatt 2002) and a short wave direction determined from the two first-order peaks (Wyatt 2012). The directional spectrum is modified, at each vector wavenumber and at each iteration, according to the difference between the radar measurement and a simulation using the directional spectrum from the previous iteration, modified by the kernel of the integral equation. The spectrum at convergence is usually very different in shape, both in frequency and direction, from the initial guess and, as will be seen, bi- and multi-modal spectra can emerge. A

further quality control is provided by a metric measuring the convergence of the inversion.

Depending on the deployment configuration there could be 10 to 100 s of directional spectra measurements across the field of view every 20 min to 1 h. Using standard techniques (see Section 3.1), this spectrum can be converted to a directional frequency spectrum (from which Fourier coefficients are obtained) and to derived parameters such as significant waveheight, peak period and direction, and wave power. A mean depth at each measurement location is needed for both the inversion and the conversion processes and best available bathymetry is used for this purpose. It is also possible to include a dynamic depth by linking the inversion to a tidal model but that has not been used in this paper.

In Section 2, the data sets are described. Section 3.1 presents the methods used, Section 3.2 the radar and buoy comparisons, and Section 4 the discussion and conclusions.

## 2 Data sets

In this paper, data from two deployments are used. Two WERA (Gurgel et al. (1999) systems were deployed on

**Table 1** Statistics of basic wave magnitude parameters

Parameter	Unit	Deployment	Buoy mean	Radar mean	cc	rms	Bias
H <sub>s</sub>	m	Norway	2.45	2.41	0.95	0.32	0.04
		Celtic Sea	2.08	2.08	0.92	0.40	0.04
T <sub>E</sub>	s	Norway	8.67	8.63	0.90	0.66	0.04
		Celtic Sea	8.37	9.33	0.72	1.58	- 0.95

**Table 2** Statistics of basic wave direction parameters

Parameter	Unit	Deployment	Vector correlation magnitude	Phase
Mean	deg	Norway	0.92	1.05
		Celtic Sea	0.90	-4.40
Peak	deg	Norway	0.64	2.38
		Celtic Sea	0.87	-4.83

islands off the Norwegian coast for a period of just over a month as a demonstration of HF radar capabilities for port management during the EuroROSE project (Wyatt et al. 2003). Two radars, separated by 10 km to up to 100 km depending on radio frequency, are needed to accurately measure both surface waves and currents. The Norwegian radars operated at a radio frequency of 27 MHz and thus had a maximum range for wave measurement of about 20 km and a maximum measurable waveheight of about 6 m. A Datawell directional waverider was installed at a location roughly 10 km offshore and some comparisons of radar bulk and spectral wave parameters with this buoy were presented in Wyatt et al. (2003). An example of a wave map from this system is shown in Fig. 2. Over most of the region mean wave direction reflects swell from the north-west. To the south, the wind waves are more dominant with winds across the region being from the south-east. The second deployment involved a Pisces radar (Wyatt et al. 2006) which was deployed at sites on the North Coast of Devon and the South Coast of Wales in the UK looking out over the Celtic Sea. This was operational over about 18 months to demonstrate the wave measurement capability. This system operates over a range of frequencies in the lower half of the HF band giving longer range and flexibility in the event of interference or to adapt to different environmental conditions. However, there are limitations in this case in low waveheights particularly for the measurement of directional characteristics (Wyatt et al. 2011). A Datawell directional waverider was deployed at 60 km from both coasts. Demonstrating the accuracy of wave measurements at this range was the main requirement of the project; high spatial resolution was not needed. Figure 2 shows an example of a wave map from this deployment during a storm. Comparisons of radar bulk and spectral parameters were carried out (Wyatt et al. 2006).

Figure 3 shows the significant waveheight comparisons for these two deployments. The Celtic Sea buoy unfortunately lost its mooring in Dec 2004 and could not be redeployed until the short break in storm conditions in mid-Jan 2005. UK Met Office model data do confirm the high significant waveheights measured by the radar in early Jan.

Statistics of the comparisons for some of the main wave parameters are presented in Tables 1 and 2. Energy period,  $T_E = \frac{\int f^{-1} E(f) df}{\int E(f) df}$ , where  $E(f)$  is the energy spectrum in  $m^2/Hz$ , is a better period comparator for the radar measurements because these have a limited upper frequency dependent on operating frequency. This formulation is dominated by the lower, energy containing frequencies and is widely used in the wave power sector. Higher ocean wave frequencies dominate in the more standard mean, or first-moment, period,  $T_1 = \frac{\int E(f) df}{\int f E(f) df}$  so, unless the buoy frequency range is limited to the same range as the radar, the radar will normally measure a higher mean period than the buoy. The low waveheight limit for the Celtic Sea data set leads to lower accuracy in period and direction unless the data are filtered to take account of this (Wyatt et al. 2011). For the data shown in the tables, periods and directions are only included if the Bragg scattering wave frequency is at least twice that of the peak frequency of a Pierson-Moskowitz spectrum (see Fig. 1),  $T_{PPM} \simeq 5\sqrt{H_s}$ , where  $H_s$  is the radar measured wavelength. During this deployment the flexible frequency was used to deal with external interference and not to account for waveheight variations which would have avoided this filtering. Note that the filtering has only been applied in these tables and not to the Fourier coefficients presented later in this paper. This provides the opportunity to explore whether some parts of the spectrum are more sensitive to this limit than others. The high waveheight limit for the Norwegian data is picked up as a quality issue during the inversion process so creates gaps in the data rather than errors. Peak direction is the direction of the wave component at the peak of  $E(f)$ . Mean direction is determined from the directional spectrum using  $\theta_m = \tan^{-1} \frac{\int \int S(f, \theta) \sin \theta d\theta df}{\int \int S(f, \theta) \cos \theta d\theta df}$  or equivalently in terms of the Fourier coefficients using  $\theta_m = \tan^{-1} \frac{\int E(f) b_1(f) df}{\int E(f) a_1(f) df}$ . Directions are compared here using vector correlation and phase difference as suggested by Kundu (1976). The phase difference is the same as the mean difference between the direction measurements.

**Fig. 4** Spectral data for Norwegian deployment on 20/02/2000 at 07:30. **a:** frequency (with a logarithmic amplitude scale) and mean direction spectra on the left, radar in black, buoy in red, directional spectra on the right using a logarithmic colour scale as shown, radar above, buoy (estimated from Fourier coefficients as discussed in the text) below. **b:** Fourier coefficients (middle two panels) and derived parameters: upper panel directional spreading from first two coefficients on left, from 2nd two coefficients on the right; lower panel skewness on the left, kurtosis on the right. **c:** spectral shape analysis as described in the text (Section 3.1) radar in shades of grey, buoy in shades of cyan. Frequencies near the peak (larger square) are shown in darker shades. In the upper frame; three standard directional distributions are shown with dashed/dotted grey lines

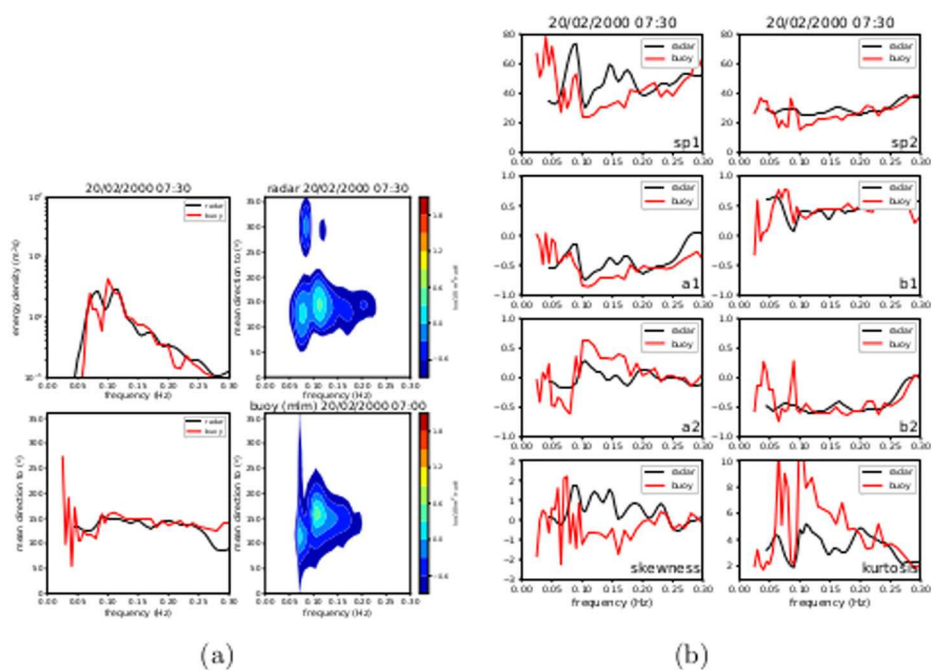


**Fig. 5** Spectral data for Norwegian deployment on 21/02/2000 at 23:30. Notation as in Fig. 4

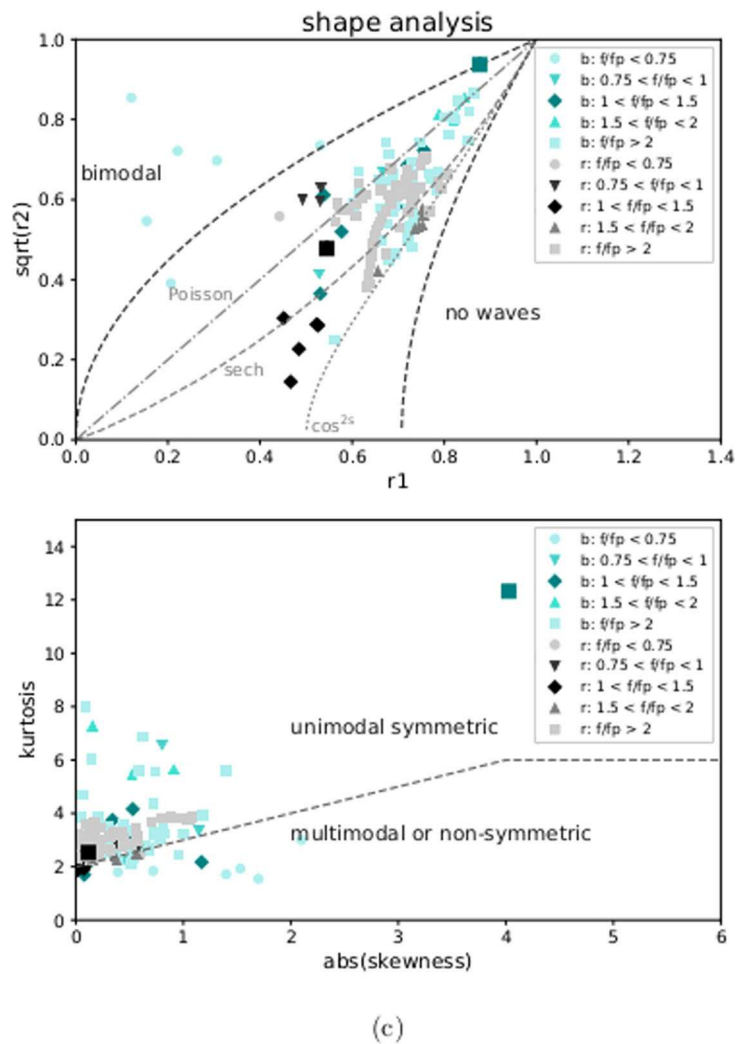
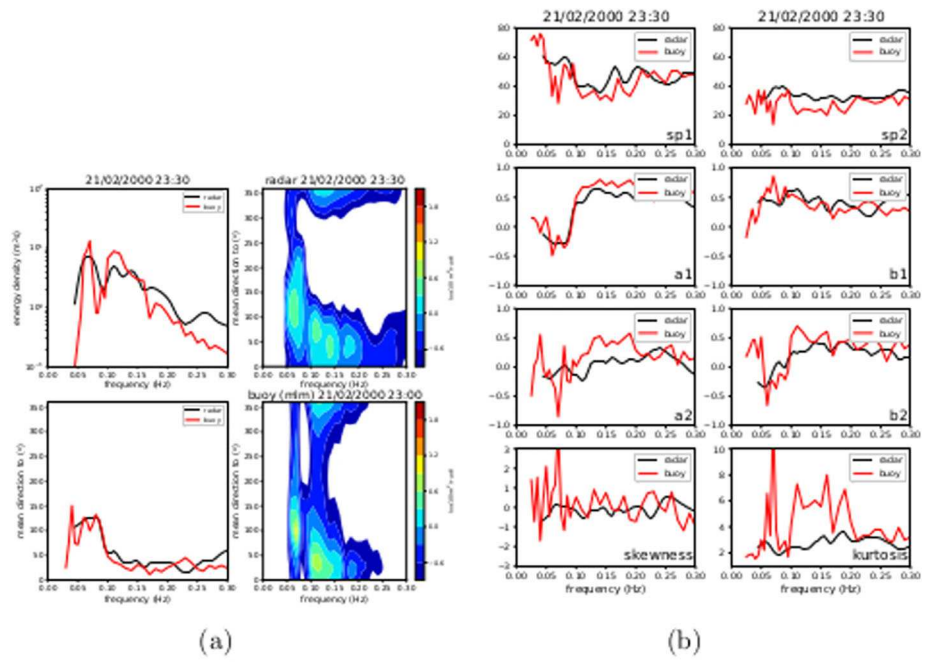




**Fig. 6** Spectral data for Celtic Sea deployment on 13/02/2005 at 02:10. Notation as in Fig. 4. Cases where the value of kurtosis falls outside the range on the yaxis are shown at the top of the plot as empty symbols and their values

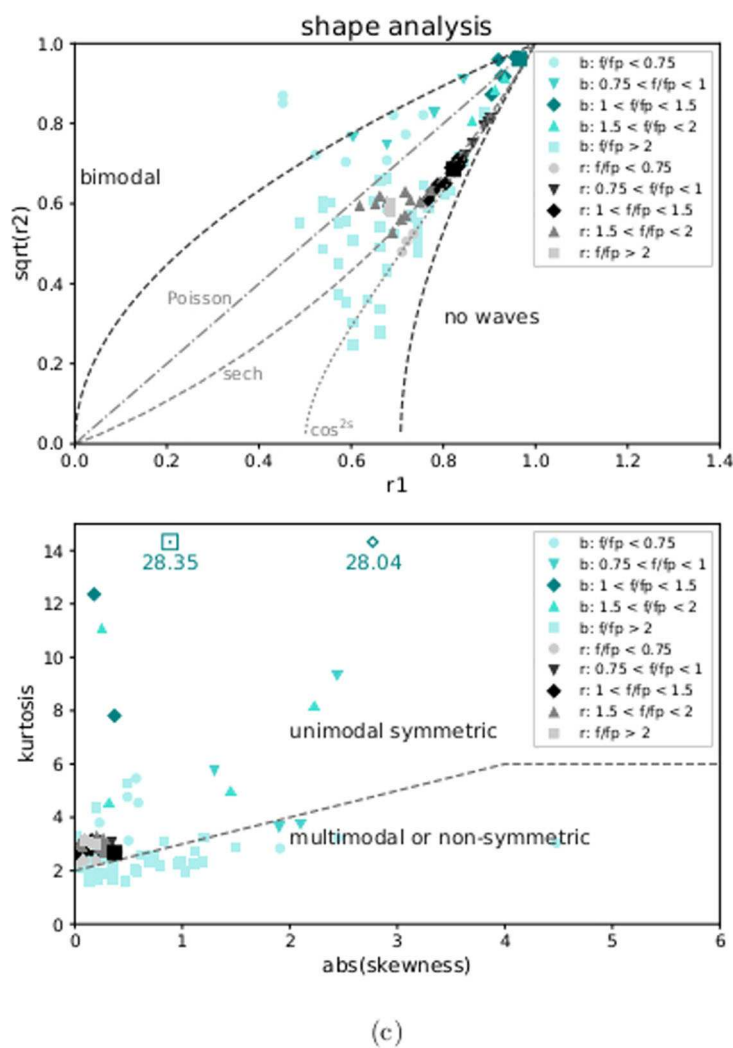
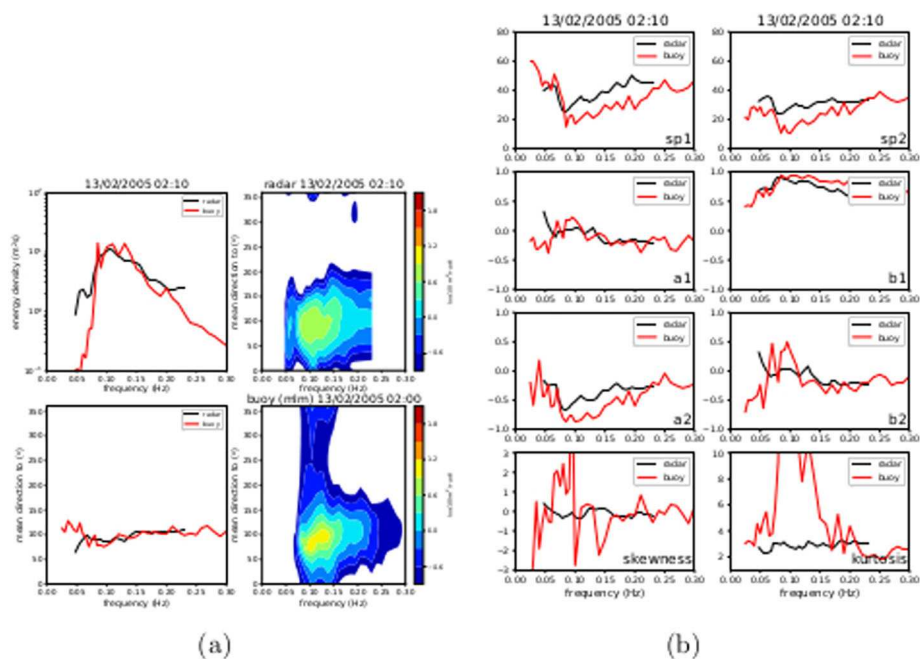
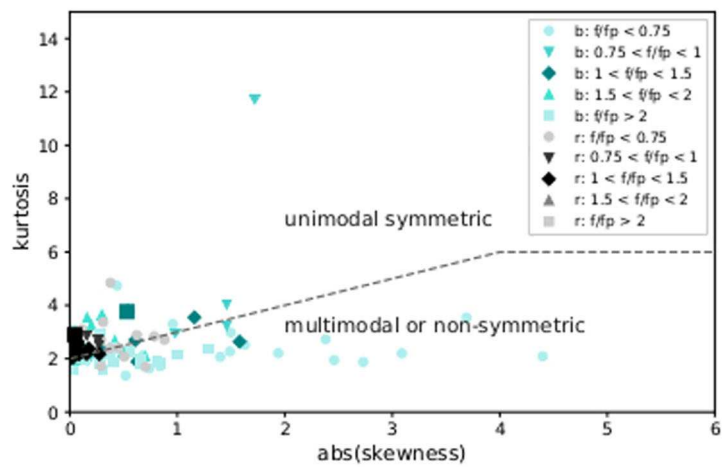
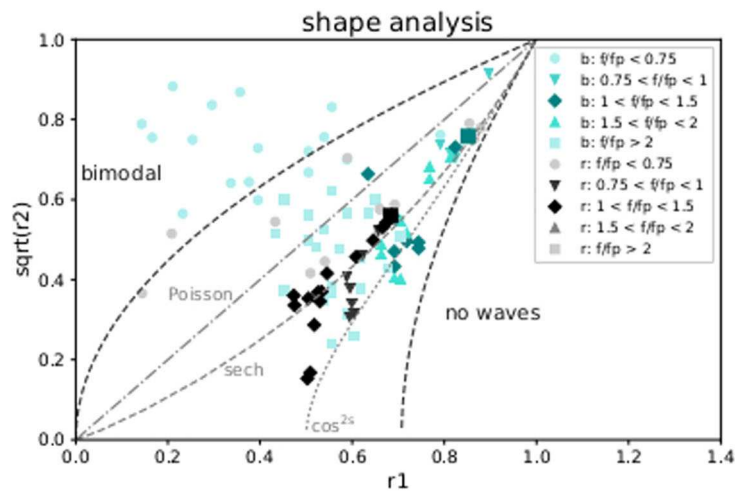
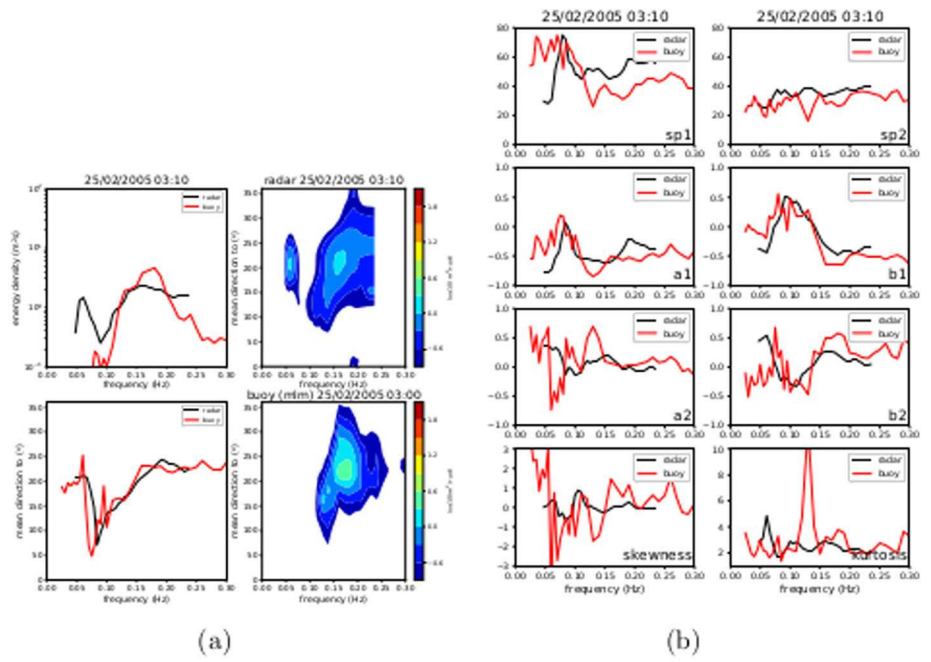


**Fig. 7** Spectral data for Celtic Sea deployment on 25/02/2005 at 03:10. Notation as in Fig. 4



(c)

## 3 Methods and comparisons

### 3.1 Methods

The output from the inversion process is an ocean wave directional spectrum,  $S(\mathbf{k})$  on a wavenumber,  $\mathbf{k}$ , grid. The grid is uniform in  $\sqrt{k}$  (where  $k = |\mathbf{k}|$ ) a convenient variable in the inversion process and is thus uniform in frequency in deep water. In this work, where depths are variable, the  $\sqrt{k}$  grid has been selected with intervals corresponding to 0.005 Hz in deep water frequency. Since all the buoy data used are provided as functions of frequency rather than wavenumber, the radar spectra have been converted to directional frequency spectra,  $S(f, \theta)$ , taking into account water depth, in the standard way, i.e.  $S(f, \theta) = \frac{dk}{df} k S(\mathbf{k})$  (Tucker 1991). Fourier coefficients have been determined from the directional frequency spectra again using standard methods (Tucker 1991). For example, writing  $S(f, \theta) = E(f)G(\theta, f)$ ,  $a_n(f) = \int_{-\pi}^{\pi} G(\theta, f) \cos n\theta d\theta$ .

Directional wave data from Datawell buoys are provided either as Fourier coefficients (estimated from the co- and quad spectra of the buoy measured time series of heave and lateral displacement) or, equivalently, as mean direction, directional spreading, skewness and kurtosis from which the Fourier coefficients can be calculated using standard methods (e.g. Kuik et al. 1998). Both forms were provided from the Norwegian buoy (allowing the conversion from one to the other to be checked) and the latter form was provided from the Celtic Sea buoy. The data used in this paper were provided with a frequency resolution of 0.005 Hz below 0.1 Hz and 0.01 Hz above. The main purpose of this paper is to compare the Fourier coefficients from the radar and buoy but a few examples of full directional spectral comparisons are also included. A number of methods have been suggested for estimating buoy directional frequency spectra from the Fourier coefficients. In this paper, the Capon (1967) method, as applied by Benoit et al. (1997), has been used to estimate the buoy spectra shown in Figs. 4, 5, 6, and 7a because this provides a smoother, less peaky spectrum, more like that from the radar. It has been found (Waters 2010) that such a model also allows for easier and more reliable partitioning of the buoy data.

In the absence of the full directional spectrum, the Fourier coefficients can be used to indicate spectral shape and the presence of bi-modality. Defining  $r_i(f) = \sqrt{a_i(f)^2 + b_i(f)^2}$ , a plot of  $\sqrt{r_2(f)}$  against  $r_1(f)$  can be used to compare data against standard directional models,

e.g.  $\cos^{2s}$  or  $\text{sech}^2$  and to identify potential bimodality (Hauser et al. 2005). Another approach to identify potential bimodality in the spectrum plots kurtosis against the absolute value of skewness both of which can be determined from the Fourier coefficients (Kuik et al. 1998). An analysis of this kind is included below in Figs. 4–7c and provide further insights into the differences between radar and buoy measurements. The relationship between  $\sqrt{r_2(f)}$  and  $r_1(f)$  for three standard directional models are shown in the figures.

### 3.2 Radar/buoy comparisons

Individual measurements of the directional spectrum and its associated Fourier coefficients are shown in Figs. 4, 5, 6 and 7a,b. Also shown are the frequency spectrum,  $E(f)$ , the mean direction, and the directional spreading at each frequency. In all cases, the radar Fourier coefficients are smoother but in reasonable agreement with those of the buoy. Small differences are amplified in the skewness and kurtosis calculations where, in general, the buoy skewness is more variable and the kurtosis is significantly higher at the spectral peak, also seen in the shape analysis plots. The inversion process requires some smoothing in both frequency and direction to ensure stability in the solution which probably accounts for this (see Green and Wyatt (2006) for a discussion about the need for, and parameters used for, the smoothing). The shape analysis in both plots in Fig. 4c shows evidence of bimodality in the radar data near the spectral peak. One explanation is that the frequency smoothing referred to above is also responsible for this evidence of directional bimodality, i.e. the individual wave components (wind-sea and swell, as seen in Fig. 4a) have more well-defined narrower frequency ranges in the buoy data than in the radar data. That is, spectra that are bimodal in frequency but not in direction at a particular frequency in the buoy data appear bimodal in direction in the radar data because of the frequency smoothing. Some must also be attributed to the evidence in both directional spectra plots, albeit clearer in the radar spectrum, of a second swell contribution well separated from the main swell and wind-sea contributions. The buoy measurements suggest bimodality at frequencies well away from the peak both above (squares) and below (circles). This is not seen in the radar data and could be indicating noise in the buoy data at these frequencies.

The directional spectra in Fig. 5a appears to show 4 different wave components although two are more merged in the buoy spectrum. The kurtosis in the buoy data is higher at all these peaks. The upper plot in the shape analysis,

**Fig. 8** Time series of energy spectra (first Fourier coefficient) for Norwegian (above) and the Celtic Sea (below) deployments. Radar measurement above, buoy below. Data gaps of 6 hours or more are shown in white; the plotting program uses the python pseudocolor routine *pcolormesh* and shorter gaps than 6 hours are thus colour-coded with the values at the end of the gap. The effect is most noticeable in the Celtic Sea data on about 20/1

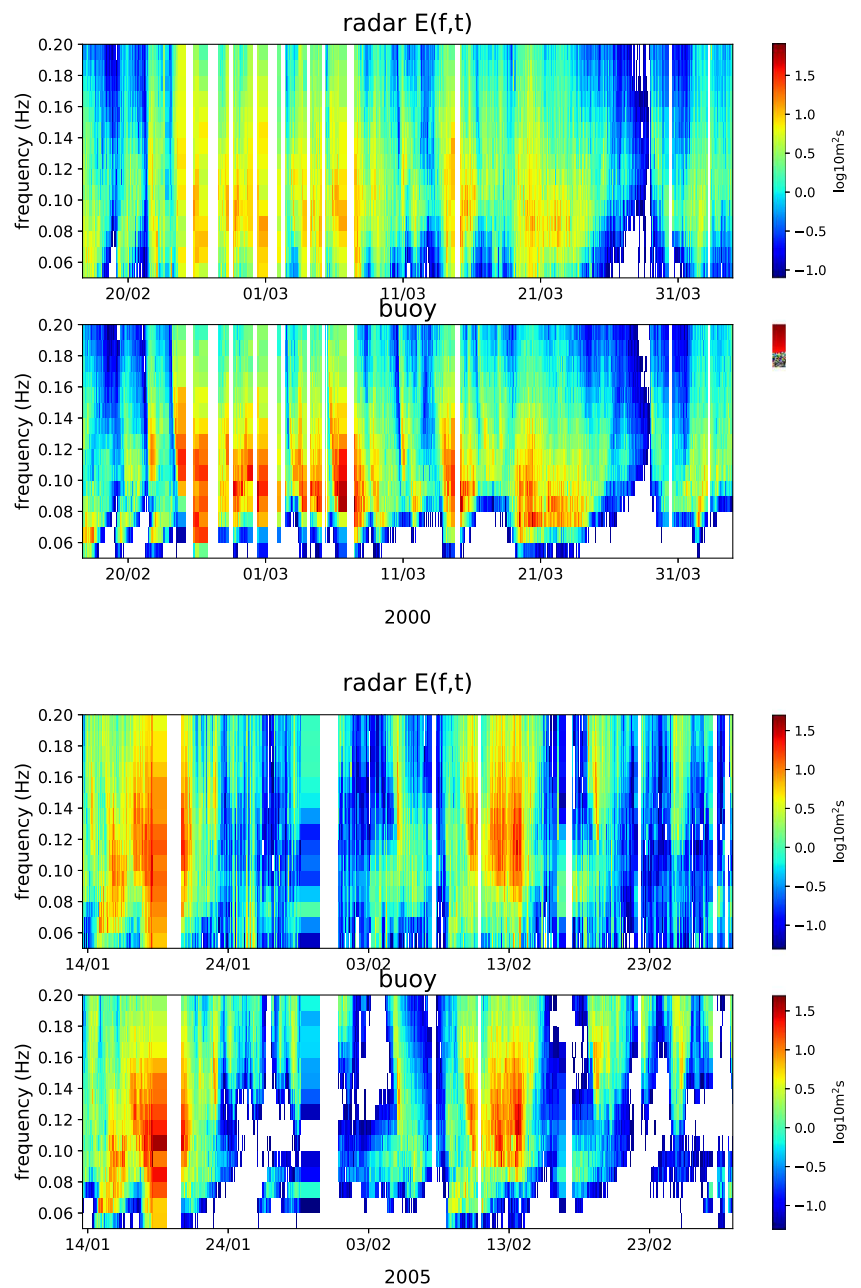
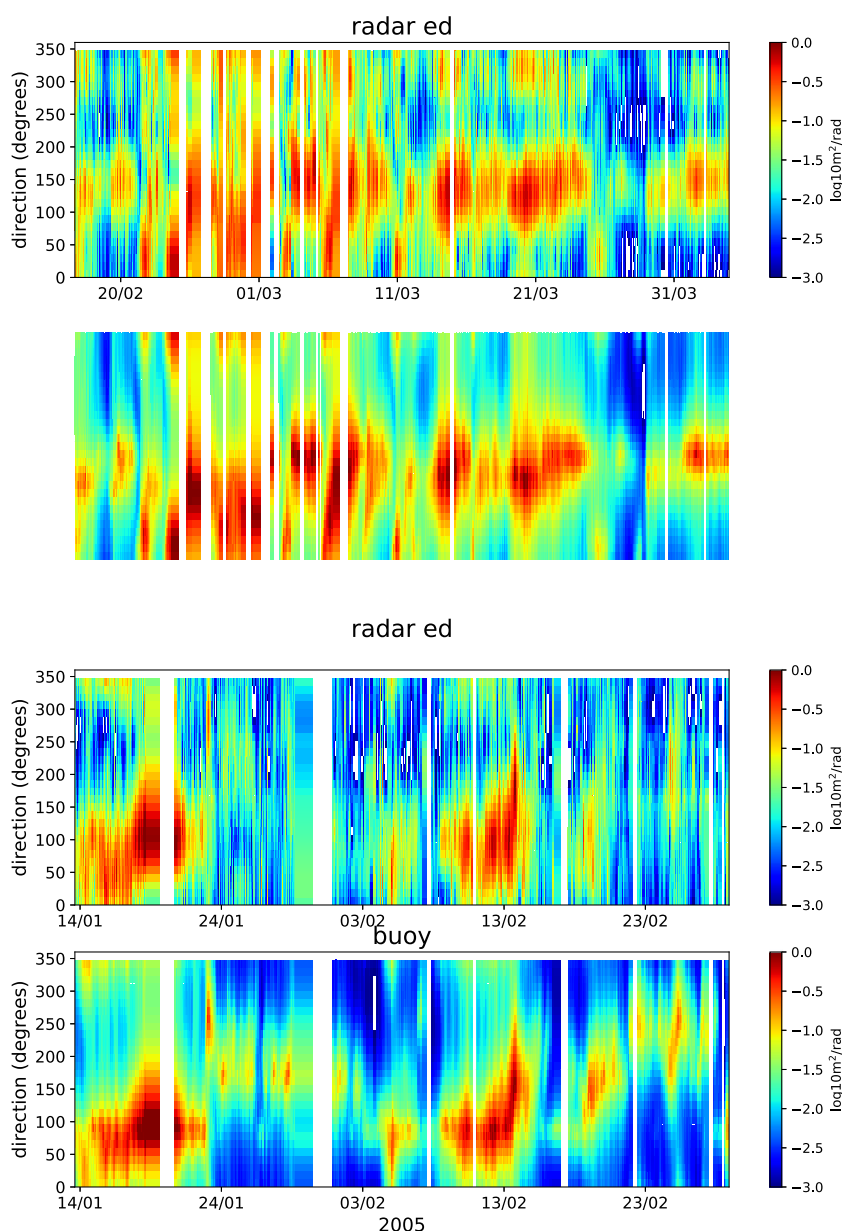


Fig. 5c, shows no bimodality in the radar data although the lower plot does indicate some multi-modality or perhaps non-symmetry near the peak. The buoy data appears to be bimodal at very low frequencies but here the amplitude is low so this again could be noise in the data. There is no conformity to standard directional shapes in either case.

The radar directional spectra in Figs. 6 and 7 whilst showing general agreement with the buoy include an extra swell component at about 0.06 Hz. These are likely to be related to ships, to antenna sidelobe signals associated with

variable surface currents across the measurement region (Wyatt et al. 2005) or to local current shear. Where one contribution to the spectrum is dominant, e.g. Fig. 6 there is some evidence in the shape analysis plots of a particular directional shape over a range of frequencies near the peak. This is particularly clear for the radar data in this case which appears to align well with a  $\text{sech}^2$  form near the peak, noting that this is indistinguishable from the  $\cos^{2s}$  form very close to the peak. In general though the data are more scattered for both types of measurement and do not conform to a

**Fig. 9** Time series of direction spectra for Norwegian (above) and the Celtic Sea (below) deployments. Radar measurement above, buoy below



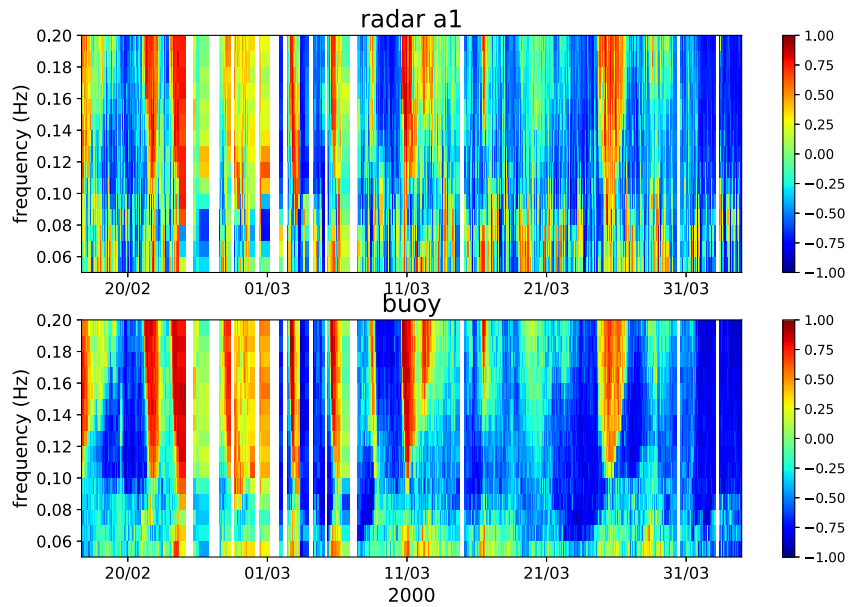
particular form. In the lower plot in Fig. 6c, the buoy is showing evidence of multi-modality or non-symmetry away from the peak whereas the upper plot shows very little evidence of bimodality. Non-symmetry is therefore likely to be the explanation and is of course consistent with the skewness shown in Fig. 6b.

The shape analysis in Fig. 7 shows some evidence that the radar data is consistent with the sech distribution. However, in this case, this may be biased by the initialisation since the peak frequency is quite high relative to the measurement range. There is no indication of bimodality in the radar

data but a slight indication of non-symmetry near the peak in the lower plot. The buoy data looks more like a  $\cos^{2s}$  shape near the peak with some evidence of bimodality at low frequencies where amplitude is low so again possibly noise in the buoy data. There is also some evidence of lack of symmetry near the peak.

For the remaining comparisons, the radar and buoy data at frequency increments of 0.01 Hz from 0.05 to 0.2 Hz are used. The first Fourier coefficient is the Energy spectrum,  $E(f) = \int_{-\pi}^{\pi} S(f, \theta) d\theta$ . This is plotted in Fig. 8 at all times when both radar and buoy provide this

**Fig. 10** Time series of the  $a_1(f)$  Fourier coefficient for Norwegian deployment. Radar measurement above, buoy below



measurement. Temporal gaps are shown as vertical white lines. The amplitudes are colour coded according to a logarithmic scale to ensure both high and low amplitudes can be compared. The temporal variation in amplitude and distribution with frequency seen in the buoy data is well captured by the radar data although, particularly for the Norwegian data the radar amplitudes are a little lower most likely due to the high operating frequency with a consequent high waveheight limit. The Celtic sea radar spectra are a little noisier at low frequencies where ship

signals and antenna sidelobes can contaminate the sea signal.

The spectra can also be integrated in frequency,  $E(\theta) = \int_{-\pi}^{\pi} S(f, \theta)df$  to give a mean amplitude in each direction and hence some indication of the directional characteristics of the wave field. This is plotted in Fig. 9 and again shows good agreement with very similar temporal variations in amplitude and distribution with direction. There are some differences in the Celtic Sea plot during periods of low waves (e.g. late Jan). This is consistent with previous work

**Fig. 11** Time series of  $b_1(f)$  Fourier coefficient for Norwegian deployment. Radar measurement above, buoy below

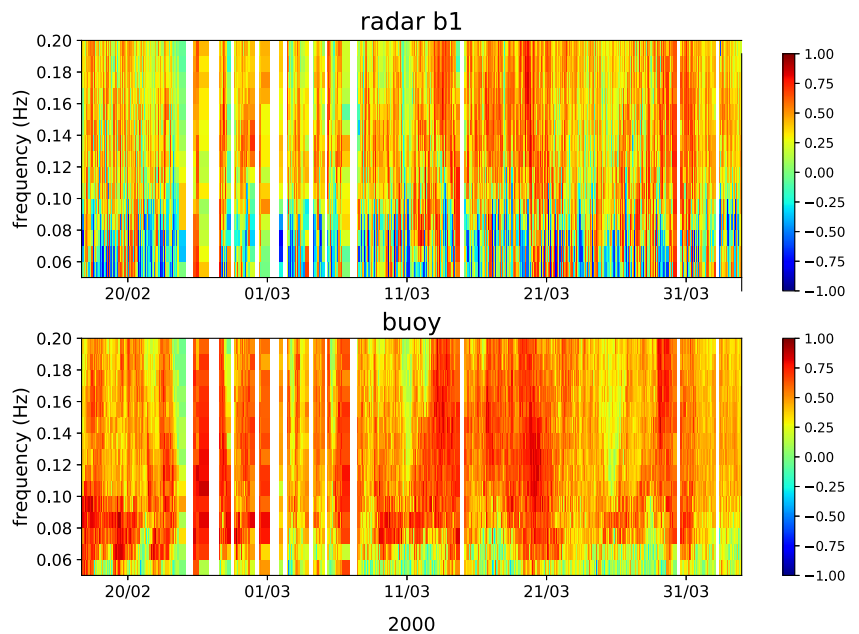
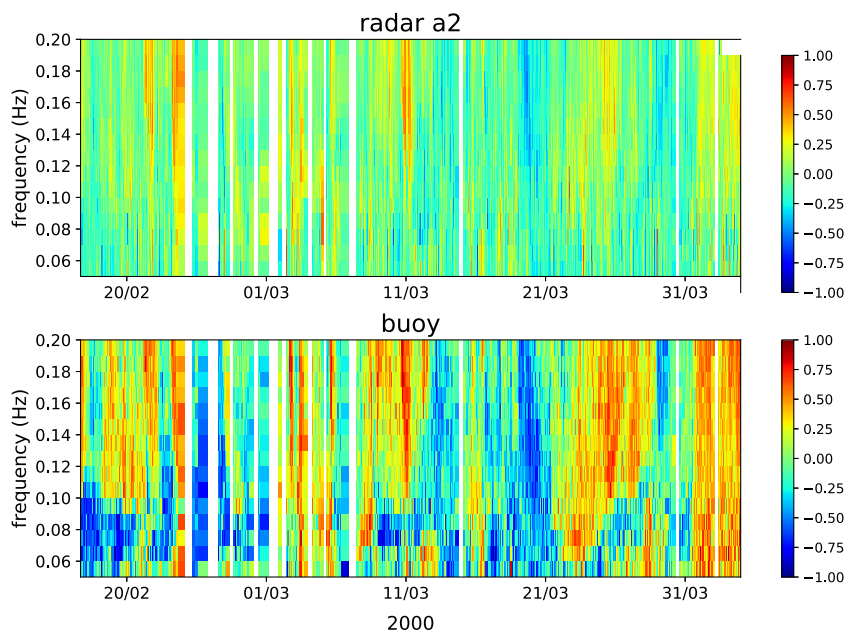


**Fig. 12** Time series of the  $a_2(f)$  Fourier coefficient for Norwegian deployment. Radar measurement above, buoy below

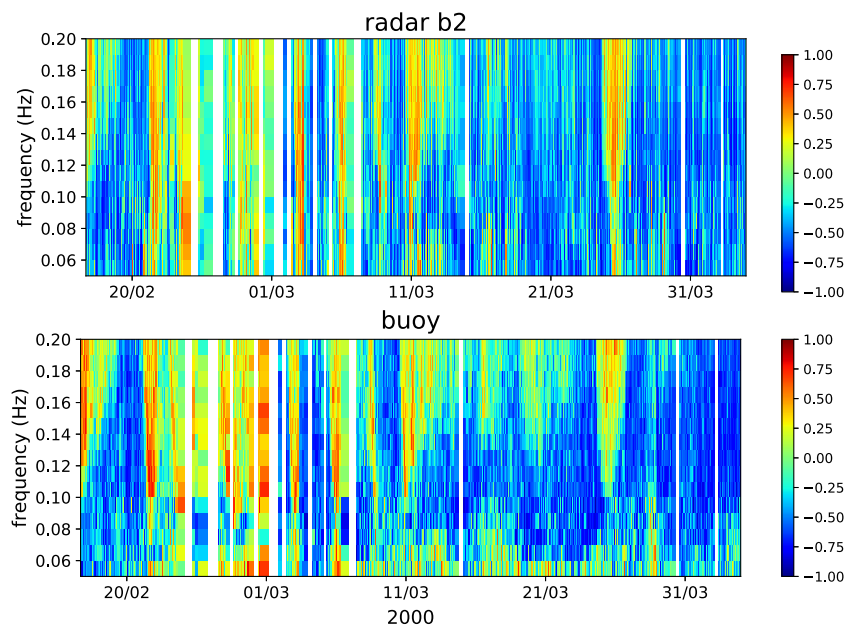


(Wyatt et al. 2011) which has shown that directions (and periods) have a higher waveheight threshold (dependent on operating frequency) for accuracy than waveheight itself. During this trial the flexibility in operating frequency that Pisces was used to avoid interference and not to adjust to waveheight conditions which would have minimised this particular problem. This has an impact on higher order Fourier coefficient comparisons. Thresholding is needed

to remove the low waveheight cases and this has not yet been done for the data shown here. Note though that there is some indication that the differences are mostly confined to low frequencies so perhaps frequency-dependent thresholding would be more appropriate.

A comparison of the four directional Fourier coefficients for the Norwegian data set are shown in Figs. 10, 11, 12, and 13. The  $a_1$  and  $b_2$  measurements are in good

**Fig. 13** Time series of  $b_2(f)$  Fourier coefficient for Norwegian deployment. Radar measurement above, buoy below



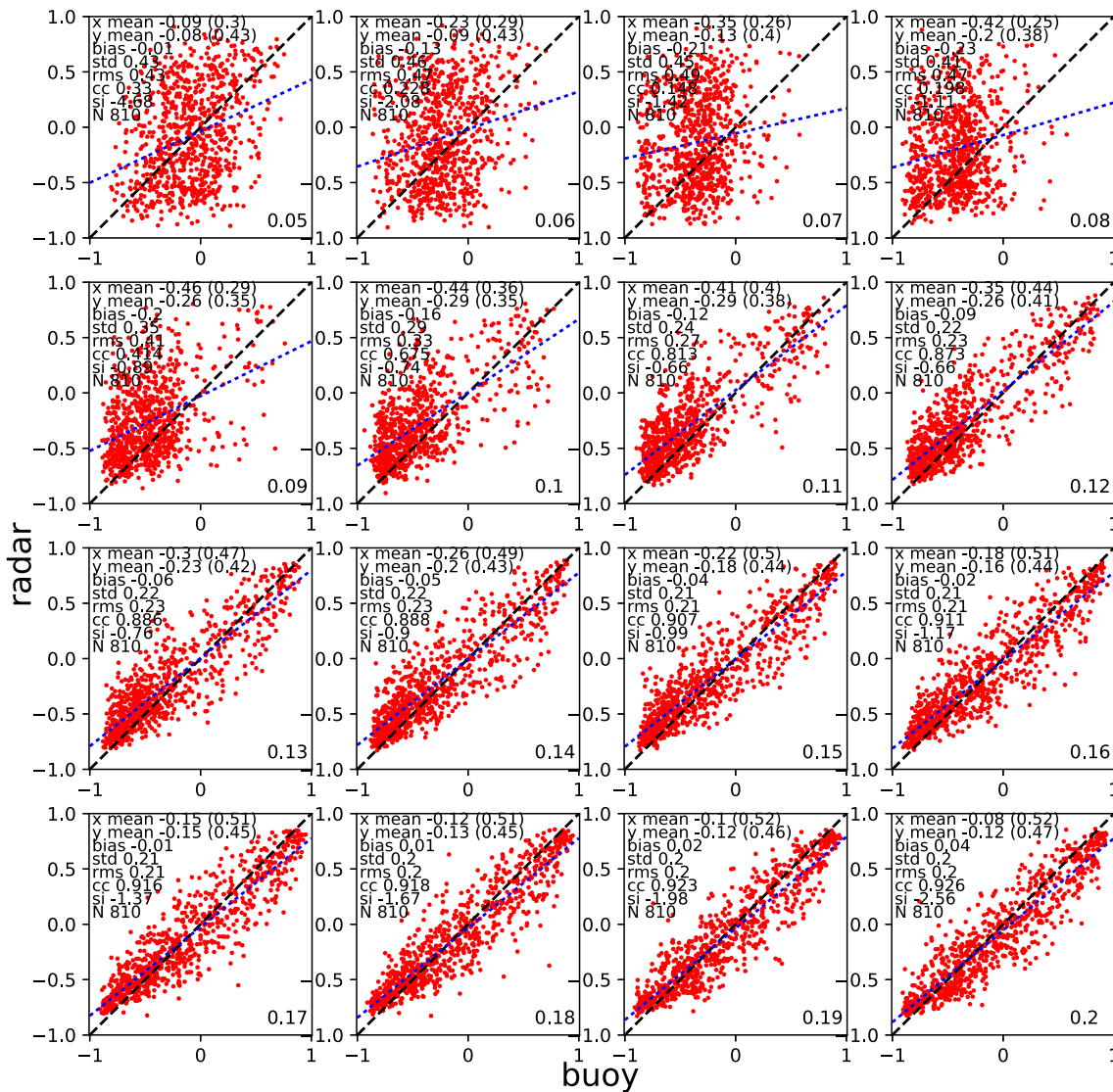


**Fig. 14** Scatter plots and statistics of the  $a_1(f)$  Fourier coefficient for Norwegian deployment. The frequency is shown in the lower right hand corner of each plot. x—buoy, y—radar. cc is the correlation coefficient; si is the scatter index but note that this is not very useful for

these data which range between  $-1$  and  $1$ ; N is the number of data pairs in the comparison

agreement although somewhat noisy at low frequencies in both measurements particularly when amplitudes are low (as seen in Fig. 8). Both radar and buoy  $b_1$  measurements show less variation with time. Similar features can be seen in the  $a_2$  measurements although the larger negative, and in some cases larger positive values in the buoy data are not seen in the radar data. These observations are confirmed in the scatter plots shown in Figs. 14, 15, 16, and 17. Correlation coefficients of over 0.9 are seen in the  $a_1$  comparison over a range of frequencies. Above

about 0.1 Hz, the standard deviations in the radar and buoy time series (shown in brackets after the means) are similar, and in each case, the rms of the comparison is lower than the individual standard deviations. The  $b_1$  coefficient varies over a smaller range and correlation coefficients are lower. Agreement is qualitatively better above about 0.1 Hz although rms differences are now similar in magnitude to the individual instrument standard deviations which is a concern. The  $a_2$  scatter plots confirm that the buoy measurements vary over a wider range than those of the



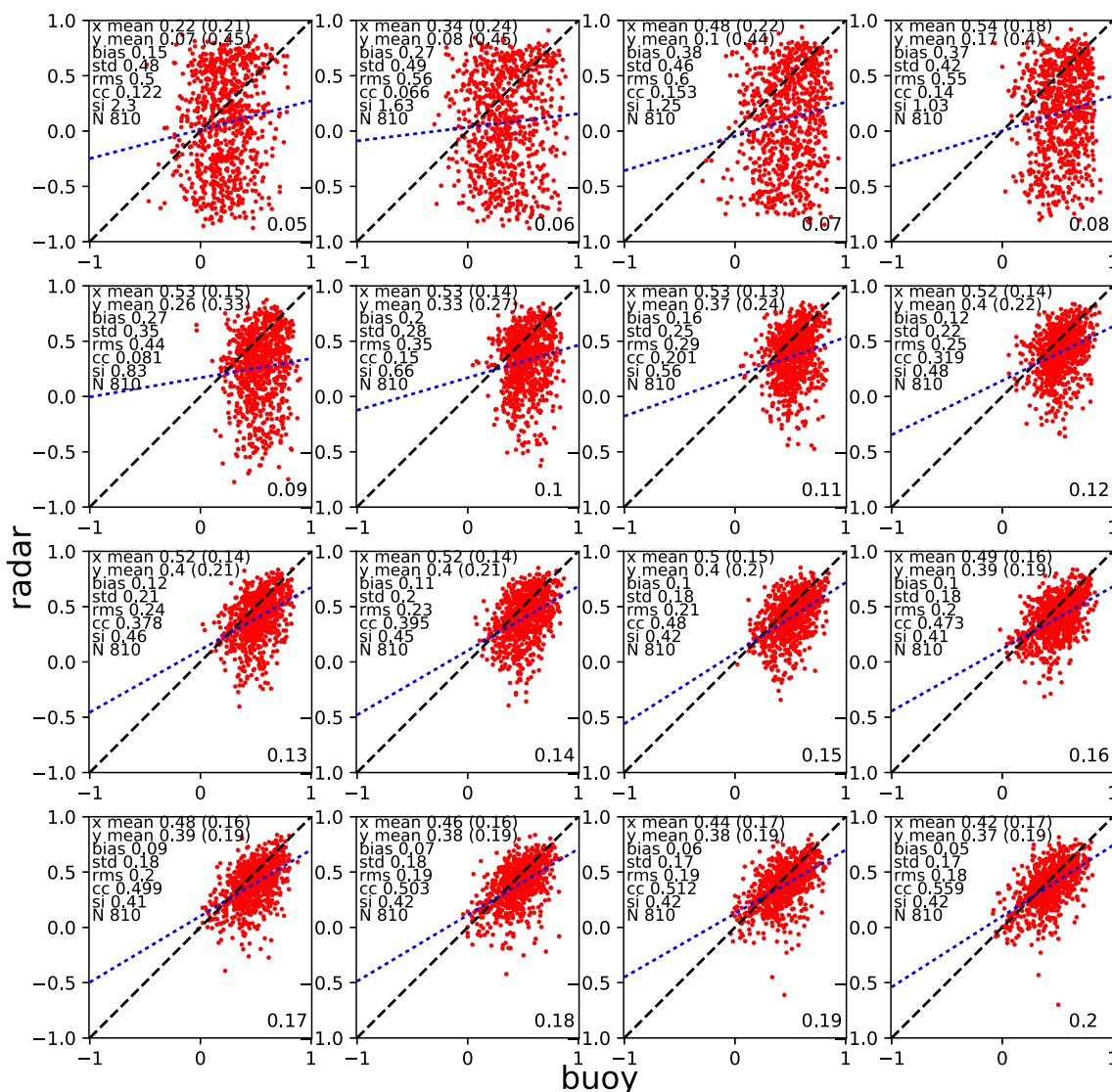


**Fig. 15** Scatter plots and statistics of  $b_1(f)$  Fourier coefficient for Norwegian deployment. Same notation as Fig. 14

radar although the correlation coefficient of over 0.6 at higher frequencies shows reasonable agreement. However, the rms in this case is higher than the standard deviation in the radar measurements although lower than that of the buoy measurements. It is possible that this Fourier coefficient is more sensitive to the inversion smoothing than the others. The correlation and rms compared to instrument standard deviations, again above about 0.1 Hz, are better for the  $b_2$  coefficient than for  $a_2$ .

Figures 18 and 19 show the directional parameters, direction and spread, derived from the first-order Fourier coefficients, i.e. mean direction =  $\tan^{-1} \frac{b_1(f)}{a_1(f)}$ , and

spread =  $\sqrt{2(1 - (a_1^2(f) + b_1^2(f))^{\frac{1}{2}})}$  both expressed in degrees. Three statistical methods are used for the direction comparisons: (a) the mean difference, its 95% confidence interval and concentration (Bowers et al. 2000); (b) the circular correlation coefficient (Fisher and Lee 1983; Fisher 1993); (c) the vector correlation and phase difference (Kundu 1976) noting that the phase difference and mean differences are equal. The statistics improve with increasing frequency above about 0.1 Hz with increasing concentrations (high values occur when scatter is low) and correlation coefficients and decreasing direction differences and their confidence intervals. The Kuik et al. (1998)

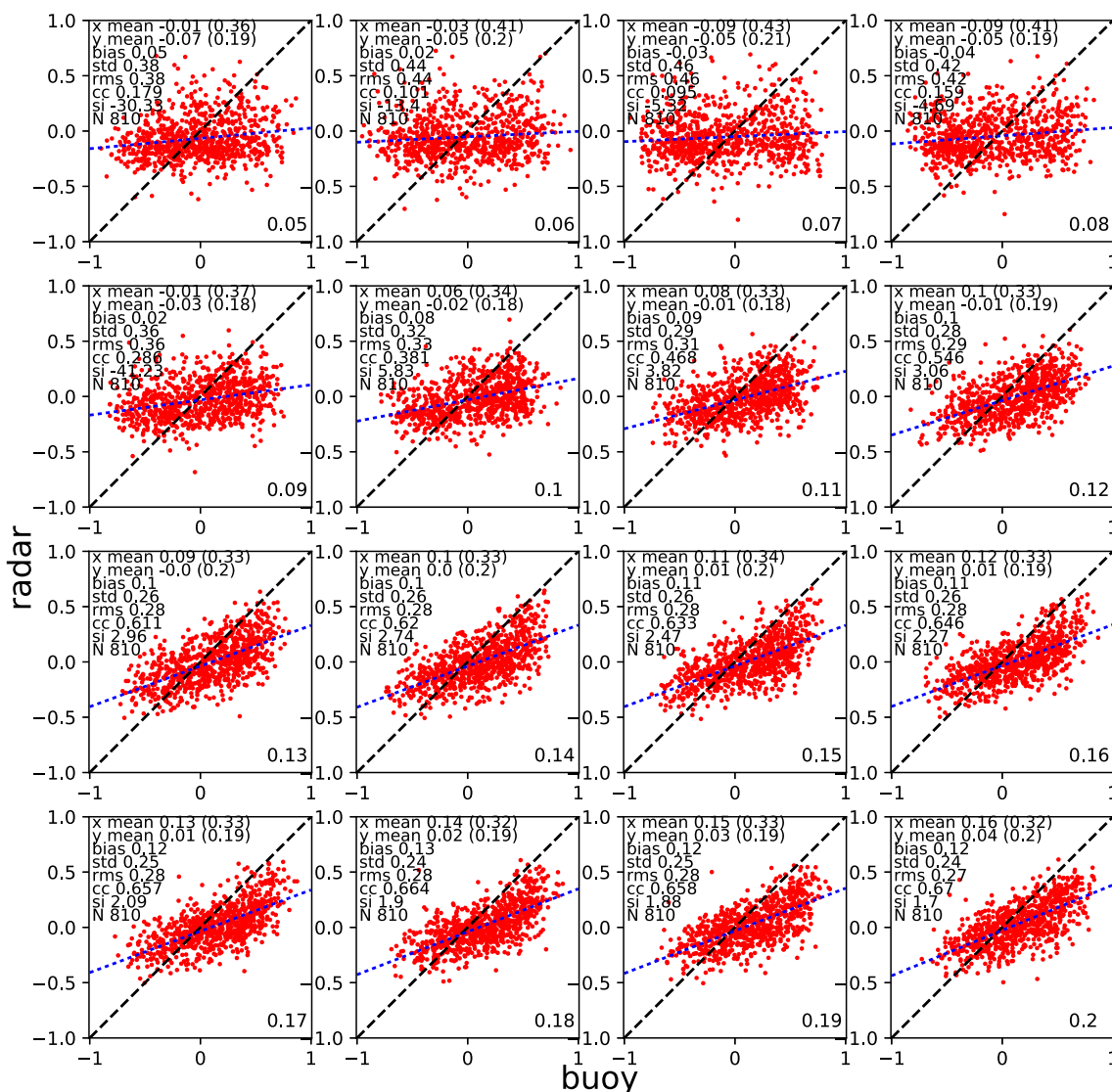


**Fig. 16** Scatter plots and statistics of the  $a_2(f)$  Fourier coefficient for Norwegian deployment. Same notation as Fig. 14

method has been used to calculate the standard deviations associated with sampling variability for the buoy direction and spread data giving mean values over the frequency range of 0.1–0.2 Hz of 4.1 deg for direction and 8.4 deg for spread. In the direction comparison, the mean difference with its confidence interval is of a similar order. The standard deviation between the spread measurements is 10–11 deg which is slightly higher than the value calculated for the buoy. This is to be expected since the radar measurement also have their own sampling variability and, in addition, there is a positive bias most likely attributable to the smoothing in the radar measurement already discussed. A

procedure for estimating the sampling variability of HF radar direction measurements was presented by Sova (1995) but these depend on radio frequency, directional spread and complexity of the directional spectrum and are not currently being used because they are difficult to apply to new deployments.

### 4 Discussion and conclusions

Although there have been a number of studies involving buoy intercomparisons which have looked at directional

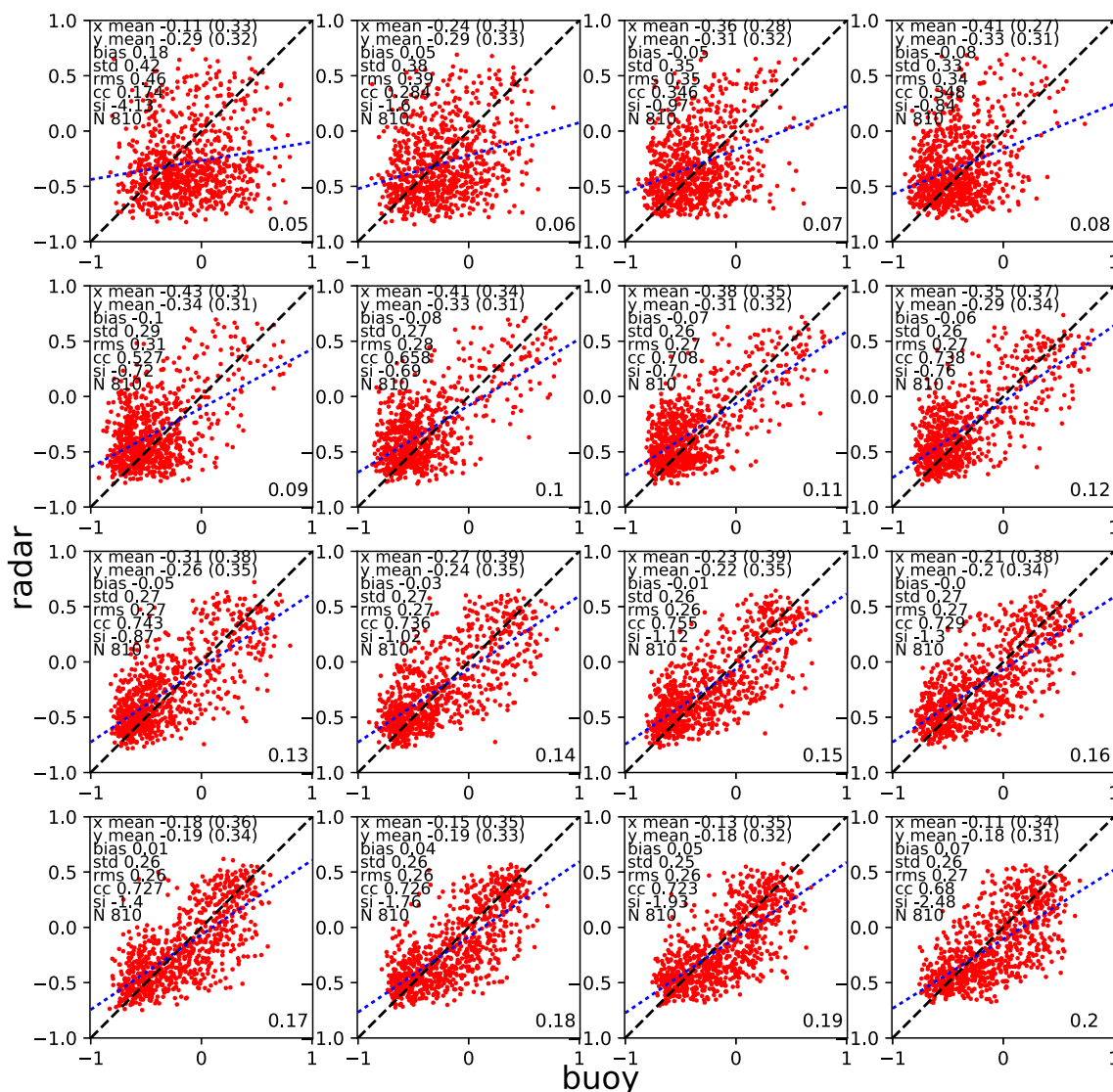


**Fig. 17** Scatter plots and statistics of  $b_2(f)$  Fourier coefficient for Norwegian deployment. Same notation as Fig. 14

parameters (e.g. Allender et al. 1989) this author has been unable to find any publications which look specifically at the Fourier coefficients although of course there are many studies looking at derived parameters such as mean direction and directional spreading. Given the stated international requirement for these coefficients perhaps such a study is needed in order to establish a benchmark for the accuracy of these parameters. In making comparisons with a directional waverider buoy and drawing conclusions about the radar data therefrom, we are therefore making the assumption that the buoy measures the true Fourier coefficients of the directional distribution. With this assumption, the results

here show that the radar tends to measure a smoother distribution of the parameters with frequency and this is attributed to the smoothing that is necessary in the inversion to stabilise the numerical solution. The temporal variation in the coefficients seen in the buoy data is well represented in the radar data although the radar  $a_2$  coefficient varies over a narrower range. The comparisons have focussed on correlation coefficients and rms differences the latter having being compared with the standard deviations in the individual buoy and radar measurements. High values of correlation coefficient and low values of rms relative to, in particular, the buoy standard deviations would imply

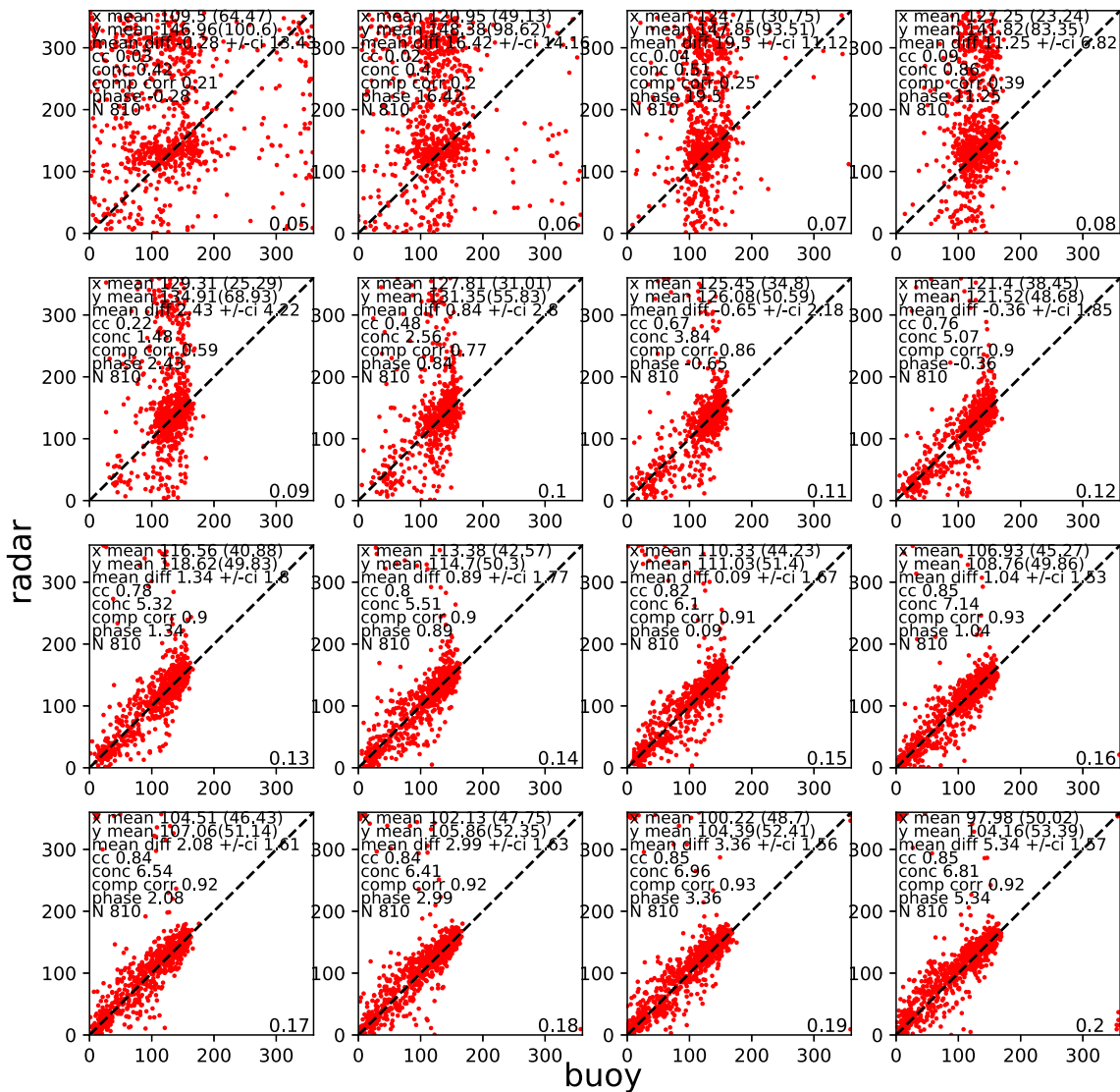


**Fig. 18** Scatter plots and statistics of mean direction in degrees for Norwegian deployment. Same notation as Fig. 14

good agreement and this has been found for the  $a_1$  and  $b_2$  coefficients. The other two coefficients appear to have been measured less reliably,  $a_2$  in particular has a much wider variance in the buoy than the radar data. However mean direction comparisons are good so perhaps the apparent lower agreement for  $b_1$  is reflecting the smaller range of values of this coefficient in both measurements rather than indicating significant radar errors.

There are significant differences in all coefficients and the associated mean direction and spread at low frequencies below about 0.1 Hz. In part, these are associated with the misinterpretation of ship signals or first-order signals coming in on the antenna sidebands as swell contributions.

There are three possible solutions to this. One is to remove the ship signals before inversion. A number of methods have been proposed for identifying ship signals in the radar data in order to provide a ship-tracking application but these are not yet routinely applied and probably not yet sufficiently robust. A second is to ensure careful calibration of the receive antenna array to minimise sidelobes although it is difficult to remove these altogether. Perhaps a more promising approach is to partition the radar spectra and use the temporal and spatial continuity of the radar data to identify and remove partitions that are unlikely to be either wind-sea or swell. Partitioning methods have been applied to HF radar data (see, e.g. Isaac and Wyatt 1997,

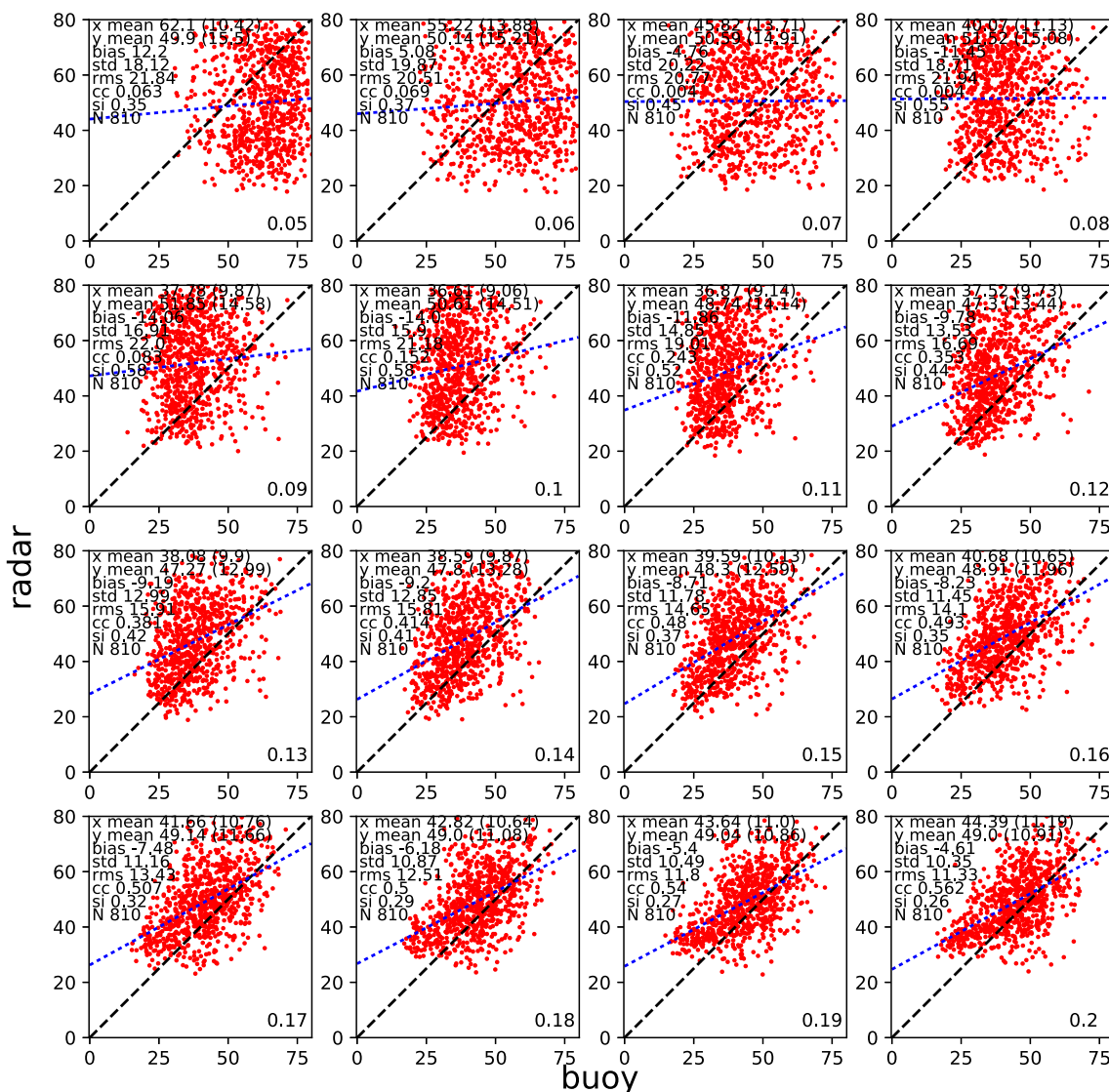


Fig. 19 Scatter plots and statistics of spread in degrees for Norwegian deployment. Same notation as Fig. 14

Waters et al. 2013) but have not yet been used in this way although some progress is being made towards this goal. The other main factor limiting the availability of good quality directional information, in regions which experience a wide range of waveheight conditions, is the low frequency limit in low sea-states and the high frequency limit in high sea-states. Having a radar that can measure over a range of frequencies responding automatically to changing conditions is the answer here although these require wideband antenna and radar hardware systems. Another explanation for the low frequency differences is that the buoy directional measurements are also noisy in this range. There is certainly less averaging in the buoy data at these frequencies. However, there is enough evidence of problems in the radar measurements at low frequencies

which need to be addressed before attributing errors to the buoys.

The shape analysis comparisons are intriguing but more work is needed to really understand the differences. There are cases showing consistency between radar and buoy and others with significant differences. In general, the radar measurements show less variation with frequency in part probably due to the smoothing in the inversion. There is some suggestions that the buoy data is noisy at frequencies well away from the peak. The two different methods appear to be consistent near the spectral peak. The more empirical (Kuik et al. 1998) method does not distinguish between multi-modality and non-symmetry, but by comparison with the other method, is likely to be indicating non-symmetry in most cases.

In both deployments discussed here, the buoy was located at a position where the angle between the look directions from the two radars is roughly 90 deg. It has been shown (Wyatt and Holden 1994) that the accuracy of the radar measurements does depend on this angle with 90 deg being optimum. A more extensive validation using in situ measurements at more locations across the radar field of view would therefore be useful to clearly establish the range and azimuthal extent of accurate data.

In conclusion, this paper has demonstrated that Fourier coefficients can be obtained from HF radar data and that they agree reasonably well with those measured with a buoy at frequencies greater than about 0.1 Hz up to 0.2 Hz, the maximum frequency analysed here. The agreement is not perfect for reasons outlined but approaches to improve the quality have been identified. Of course the radar is making these measurements over wide areas of the coastal ocean so can measure spatial as well as temporal variations in these quantities. Waves vary in the coastal environment due to changes in depth and coastal topography with associated variations in current and in wind and a spatial picture with good but possibly lower accuracy may be more useful for some applications.

**Acknowledgements** The Norwegian data were obtained during the EU-funded EuroROSE project and we thank Klaus-Werner Gurgel and all of the EuroROSE team for their contributions. The Pisces data was provided by Neptune Radar and collected during a project funded by DEFRA and the UK Met Office. The buoy data for this experiment have been provided by CEFAS. Some of these data sets were processed and provided by Seaview Sensing Ltd. Referees made a number of very useful suggestions that have improved the paper.

**Open Access** This article is distributed under the terms of the Creative Commons Attribution 4.0 International License (<http://creativecommons.org/licenses/by/4.0/>), which permits unrestricted use, distribution, and reproduction in any medium, provided you give appropriate credit to the original author(s) and the source, provide a link to the Creative Commons license, and indicate if changes were made.

## References

- Allender J, Audunson T, Barstow SF, Bjerken S, Krogstad HE, Steinbakke P, Vardel L, Borgman LE, Graham C (1989) The WADIC project: a comprehensive field evaluation of directional wave instrumentation. *Ocean Eng* 16:505–536
- Barrick D, Weber BL (1977) On the nonlinear theory for gravity waves on the ocean's surface. Part II: Interpretation and applications. *J Phys Oceanogr* 7:11–21
- Barrick DE (1972) First order theory and analysis of MF/HF/VHF scatter from the sea. *IEEE Trans Antennas Prop* 20:2–10
- Barrick DE (1972) Remote sensing of sea state by radar. In: Derr VE (ed) *Remote sensing of the troposphere*, chap 12. Washington, DC GPO
- Benoit M, Frigard P, Schaffer HA (1997) Analysing multidimensional wave spectra: a tentative classification of available methods. In: Seminar on multidimensional waves and their interaction with structure, pp 131–158
- Bowers JA, Morton ID, Mould GI (2000) Directional statistics of the wind and waves. *Appl Ocean Res* 22:13–30
- Capon J (1967) Multidimensional maximum-likelihood processing of a large aperture seismic array. *Proc IEEE* 55:192–211
- Donelan MA, Hamilton J, Hui WH (1985) Directional spectra of wind-generated waves. *Philos Trans R Soc London A* 315:509–562
- Fisher NI (1993) *Statistical analysis of circular data*. Cambridge University Press, Cambridge
- Fisher NI, Lee AJ (1983) A correlation coefficient for circular data. *Biometrika* 70:327–332
- Green JJ, Wyatt LR (2006) Row-action inversion of the Barrick-Weber equations. *J Atmos Ocean Technol* 23:501–510
- Gurgel KW, Antonischki G, Essen HH, Schlick T (1999) Wellen radar (WERA): a new ground-wave HF radar for ocean remote sensing. *Coast Eng* 37:219–234
- Hauser D, Kahma K, Krogstad HE, Lehner S, Monbaliu JAJ, Wyatt LR (eds) (2005) *Measuring and analyzing the directional spectra of ocean waves*, vol EUR 21367. Luxembourg Office for Official Publications of the European Communities, Luxembourg
- Hisaki Y (1996) Nonlinear inversion of the integral equation to estimate ocean wave spectra from hf radar. *Radio Sci* 31:25–39
- Howell R, Walsh J (1993) Measurement of ocean wave spectra using narrow beam HF radar. *IEEE J Ocean Eng* 18:296–305
- Isaac F, Wyatt LR (1997) Segmentation of high-frequency radar-measured directional wave spectra using the Voronoi diagram. *J Atmos Ocean Technol* 14:950–959
- Kuik AJ, van Vledder GP, Holthuijsen LH (1998) A method for the routine analysis of pitch-and-roll buoy wave data. *J Phys Oceanogr* 18:1020–1034
- Kundu PK (1976) Ekman veering observed near the ocean bottom. *J Phys Oceanogr* 6:238–242
- Lipa B, Barrick D, Alonso-Martirena A, Fernandez M, Ferrer MI, Nyden B (2014) Braham project high frequency radar ocean measurements: currents, winds, waves and their interactions. *Remote Sens* 6:12,094–12,117
- Lipa B, Barrick DE (1986) Extraction of sea state from hf radar sea echo: Mathematical theory and modelling. *Radio Sci* 21:81–100
- Lipa BJ (1977) Derivation of directional ocean-wave spectra by inversion of second order radar echoes. *Radio Sci* 12:425–434
- Long RM, Barrick D, Largier JL, Garfield N (2011) Wave observations from central california: Seasonal systems and in situ wave buoys. *J Sensors* 2011:1–18
- Hashimoto N, Tokuda M (1999) A bayesian approach for estimating directional spectra with hf radar. *Coast Eng J* 41:137–149
- Pierson WJ, Moskowitz LA (1964) Proposed spectral form for fully developed wind seas based on the similarity theory of S. A. Kitaigorodskii. *J Geophys Res* 69:5181–5190
- Sova MG (1995) *The sampling variability and the validation of high frequency wave measurements of the sea surface*. Ph.D. thesis, University of Sheffield, Sheffield
- Swail V, Jensen R, Lee B, Turton J, Thomas J, Gulev S, Yelland M, Etala P, Meldrum D, Birkemeier W, Burnett W, Warren G (2010) Wave measurements, needs and developments for the next decade. In: Hall J, Harrison D, Stammer D (eds) *Proceedings of OceanObs'09: Sustained Ocean Observations and Information for Society*, Vol. 2. Noordwijk, The Netherlands, European Space Agency, 999-1008. (ESA Special Publication, WPP-306)
- Tucker MJ (1991) *Waves in ocean engineering measurement, analysis, interpretation*. Chichester

- USACE (2009) A national operational wave observation plan. [https://cdn.ioos.noaa.gov/media/2017/12/wave\\_plan\\_final\\_03122009.pdf](https://cdn.ioos.noaa.gov/media/2017/12/wave_plan_final_03122009.pdf)
- Waters J (2010) Data assimilation of partitioned HF radar wave data into wave models. Ph.D. thesis, University of Sheffield, Sheffield
- Waters J, Wyatt L, Wolf J, Hines A (2013) Data assimilation of partitioned HF radar wave data into wavewatch III. *Ocean Model* 72:17–31. <https://doi.org/10.1016/j.ocemod.2013.07.003>
- Wyatt LR (1990) A relaxation method for integral inversion applied to HF radar measurement of the ocean wave directional spectrum. *Int J Remote Sens* 11:1481–1494
- Wyatt LR (2000) Limits to the inversion of HF radar backscatter for ocean wave measurement. *J Atmos Ocean Technol* 17:1651–1666
- Wyatt LR (2002) An evaluation of wave parameters measured using a single HF radar system. *Can J Remote Sens* 28:205–218
- Wyatt LR (2012) Shortwave direction and spreading measured with HF radar. *J Atmos Ocean Technol* 29:286–299
- Wyatt LR, Green JJ, Gurgel KW, Borge JCN, Reichert K, Hessner K, Günther H, Rosenthal W, Saetra O, Reistad M (2003) Validation and intercomparisons of wave measurements and models during the euroROSE experiments. *Coast Eng* 48:1–28
- Wyatt LR, Green JJ, Middleditch A (2011) HF radar data quality requirements for wave measurement. *Coast Eng* 58:327–336
- Wyatt LR, Green JJ, Middleditch A, Moorhead MD, Howarth J, Holt M, Keogh S (2006) Operational wave, current and wind measurements with the Pisces HF radar. *IEEE J Ocean Eng* 31:819–834
- Wyatt LR, Holden G (1994) Limits in direction and frequency resolution for HF radar ocean wave directional spectra measurements. *The Global Atmosphere-Ocean System* 2:265–290
- Wyatt LR, Liakhovetski G, Graber H, Haus B (2005) Factors affecting the accuracy of HF radar wave measurement. *J Atmos Ocean Technol* 22:844–856